Studia Quaternaria, vol. 42 (2025): 111–126
DOI: 10.24425/sq.2025.157455

SEASONAL AND SPATIAL VARIATIONS OF THE PLIO-QUATERNARY AQUIFER'S WATER QUALITY IN *SIDI SMAIL* PLAIN, NORTHWESTERN TUNISIA

Ghofrane Charrada[1*], Brahim Askri[1], Wissem Hemdi[2], Boulbaba Louhichi[2], Noureddine Hamdi[2,3]

[1] *University of Gabès, Research Unit of Modeling in Civil Engineering and Environment, National Engineering School of Gabès, Tunisia; e-mails: ghofranecharrada@gmail.com (G. Charrada); askrib@yahoo.com (B. Askri)*
[2] *University of Gabès, Higher Institute of Water Sciences and Techniques of Gabes, Tunisia; e-mails: wissemhemdi@yahoo.fr (W. Hemdi); boulbabalouhichii@gmail.com (B. Louhichi); nouryhamdi@gmail.com (N. Hamdi)*
[3] *Laboratory of Composite Materials and Clay Minerals, National Center of Research in Materials Sciences (CNRSM), B.P.73-8020, Soliman, Tunisia*
** corresponding author*

Abstract:
Groundwater salinization and contamination by nitrates represent two major environmental threats that can deteriorate its quality and pose serious health problems in many regions worldwide. This study aims to investigate the groundwater quality and to evaluate its suitability for drinking and irrigation purposes in the agricultural plain of Sidi Smail (northwestern Tunisia) using statistical, modeling, and GIS tools. A total of 59 groundwater samples and four surface water samples were collected in the autumn transition (October 2021) and the dry summer season (August 2022) and analyzed for pH, electrical conductivity (EC), total dissolved solids (TDS), and major ion concentrations. The results indicated that the majority of the groundwater samples were brackish/saline with an average TDS value of 2.225 mg/L in the autumn and 2.381 mg/L in the summer. The little increase in TDS values of surface and groundwater in the last season was attributed to the increase of evaporative demand and the decrease of rainfall amount. The groundwater mineralization in the plain had a significant spatial variability. The highest TDS values and concentrations of major ions were recorded in the southern sector of the plain due to the dissolution of Triassic evaporites deposits, while the lowest values were observed in the northern part of the plain likely due to the groundwater dilution caused by the infiltration of rainfall and seepage of surface water through faults of Ypresian karstic formations. The WQI values of groundwater ranged from 45 to 281, classifying the samples into four categories. In the autumn, 3% of samples were excellent, 36% good, 47% poor, and 14% very poor. In the season, 37% of samples were good, 43% poor, and 20% very poor. The integration of geochemical tools, statistical analyses, the water quality index (WQI), and GIS-based mapping constitutes a robust and comprehensive framework for assessing factors influencing the seasonal and spatial variations in sub-humid to semi-arid regions subjected to intensive agricultural practices. The results of this study highlight the urgent global need for the rational and controlled use of fertilizers to safeguard groundwater resources from nitrate contamination.

Key words: Groundwater quality, dissolution-precipitation, agricultural plain, northwester Tunisia.

Manuscript received 11 August 2025, accepted 24 November 2025

INTRODUCTION

Groundwater is the principle water supply source for domestic, agricultural, and industrial activities in many arid and semi-arid regions worldwide (Karunanidhi *et al.*, 2021). It is expected that groundwater provides about 73% of global fresh water (Abanyie *et al.*, 2023). However, the climate change and the improper management of ground-

water had resulted in a significant drop in water table levels (Davamani *et al.*, 2024; Rouhani *et al.*, 2025). Additionally, recurrent irrigation events using brackish or saline water have facilitated groundwater pollution through the leaching of soluble salts and nitrates accumulated in the plant root zone. Groundwater contamination by nitrate worsens in many regions due to leakage from sanitation systems (Chaudhary *et al.*, 2025). Groundwater salinization harms food production by increasing the soil salinity and thus enhancing the soil osmotic pressure, while the excessive nitrate levels in the groundwater are becoming a major public health issue across the globe (Hamdi *et al.*, 2018; Nyika *et al.*, 2024). Recently, the water quality has become an important focus due to its strong link not only to human health but also to agricultural production. Effective management of water resources under climate change and environmental challenges require a clear understanding of the spatial distribution of water quality patterns and governing processes (Arslan, 2012; Agoubi *et al.*, 2013; Lissir *et al.*, 2025). Periodic changes in groundwater quality can be attributed to temporal changes in recharge water quality, hydrological processes, climatic factors, and human activities mainly in the agricultural sector (Abbasi *et al.*, 2024; Hadroug *et al.*, 2025). In many agricultural regions worldwide, the degradation of groundwater quality due to high levels of salinity and nitrates has become a growing concern (Bouita *et al.*, 2021; Hamdi *et al.*, 2022; Sanad *et al.*, 2024). To better understand the origins and hydrochemical processes responsible for these twin issues, researchers have employed a variety of tools and approaches including the Piper diagram, the saturation indices (SI), the Gibbs plot, and the isotopic approach (Maman Hassan and Fırat Ersoy, 2022; Benyoussef *et al.*, 2024).These tools and methods provide valuable insights into the chemical characteristics, sources, and evolution of groundwater quality. In recent years, growing concern over groundwater quality has led to the development of several quantitative indicators to assess pollution levels and associated health risks. Among these, the Water Quality (WQI) models are widely used to assess the water quality (surface and groundwater) and its suitability for drinking purpose (Nong *et al.*, 2020; Uddin and Olbert, 2021). These models use aggregation functions to combine several physicochemical data from different times into a single value (Nives, 1999). Moreover, many diagrams such as the USSL diagram and several index models such as the Irrigation Water Quality Index (IWQI) were used to assess the suitability of water for irrigation use by its classification based on two or more hydrochemical parameters or the IWQI value (Singh *et al.*, 2018). Using the IWQI, Batarseh *et al.* (2021) demonstrated that 52% of the groundwater samples collected in Abu Dhabi Emirate are under severe irrigation restriction.

About 82% of Tunisia's surface water is provided by the transboundary Medjerda River, which originates in the Tell Atlas in northeastern Algeria (Gaaloul *et al.*, 2023). The river's watershed has been severally impacted by the climate change, which has depleted the surface water resources and increased their mineralization (Kadir *et al.*, 2020; Rajosoa *et al.*, 2022; Ben Ayed *et al.*, 2022). These factors have decreased the agricultural productivity and the food supply, prompting the authorities to exploit the available groundwater resources within the watershed to compensate the shortage of water, particularly in the agro-industrial sectors. However, this strategy has led to significant groundwater depletion and deterioration in water quality (Belhadj *et al.*, 2025). Under persistent dry climatic conditions, farmers in the Medjerda watershed have increased fertilizer application to enhance crop growth and yields. However, the excess of nitrates can dissolve in rainwater or irrigation water, leach down through the soil, and reach the groundwater, thereby exacerbating its pollution (Macdonald *et al.*, 2020). Additional sources of nitrates resulting from leaking septic systems, damaged sewer pipelines, and untreated sewage discharge may deteriorate further the groundwater quality. Given the multiple sources of nitrate pollution and salinization in groundwater, it is essential to investigate the hydrochemical mechanisms governing the groundwater quality in the Medjerda watershed to ensure effective conservation and sustainable water resources management. Sidi Smail plain is one of the principal agricultural zones within the Medjerda watershed. Over the past two decades, groundwater quality in this plain has experienced alarming signs of degradation, primarily due to increasing salinization and elevated nitrate concentrations. The present study aims to investigate the groundwater quality and to evaluate its suitability for drinking and irrigation purposes in Sidi Smail plain. The objectives are to: (1) assess the hydrochemical processes governing the groundwater quality, (2) depict the factors influencing the seasonal and spatial variations of the groundwater quality, and (3) evaluate the groundwater suitability for drinking and irrigation purposes. Understanding the temporal and spatial variations of the groundwater quality in Sidi Smail plain will help the deciders, the farmers and the stakeholders to manage properly the groundwater resources.

STUDY REGION

Sidi Smail plain is located in southwestern Béja governorate, in the northwest of Tunisia. It has an area of about 400 km^2 in the middle-valley of the Medjerda basin (Fig. 1). The multi-year (1991–2020) climatic data recorded by the National Institute of Meteorology in Tunisia indicates that the average monthly inter-annual air temperature fluctuates between 8.6°C in January and 27.4°C in August with a mean of 17.2°C and a standard deviation of 6.9°C, whereas the monthly inter-annual precipitation varies between 6.6 mm in July and 86.6 mm in January with a mean of 49.0 mm and a standard deviation of 26.3 mm (Fig. 2). A well-defined dry season extending from May to August, characterized by high temperatures and minimal precipitation followed by a wet season between November and March, when temperatures decrease and rainfall increases The mean inter-annual precipitation and potential evapotranspiration are about 530 and 900 mm/year, re-

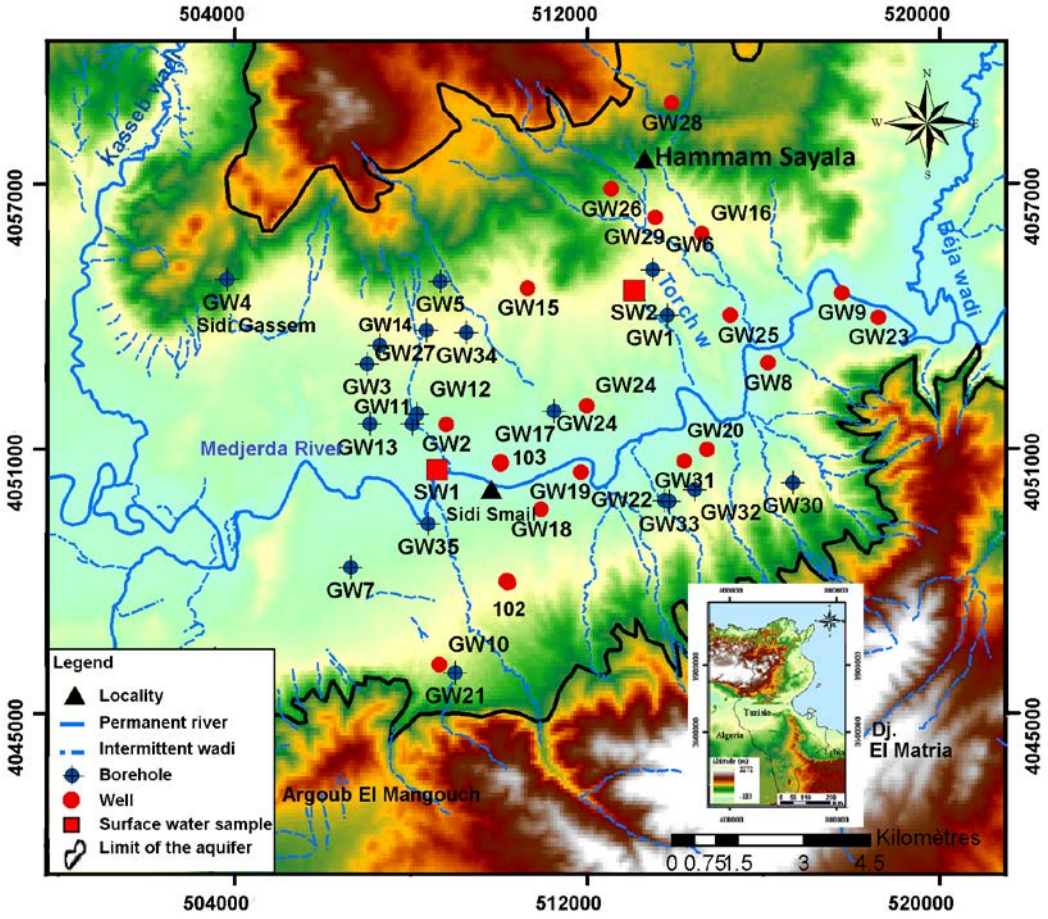

Fig. 1. Location of the study area (*Sidi Smail* plain).

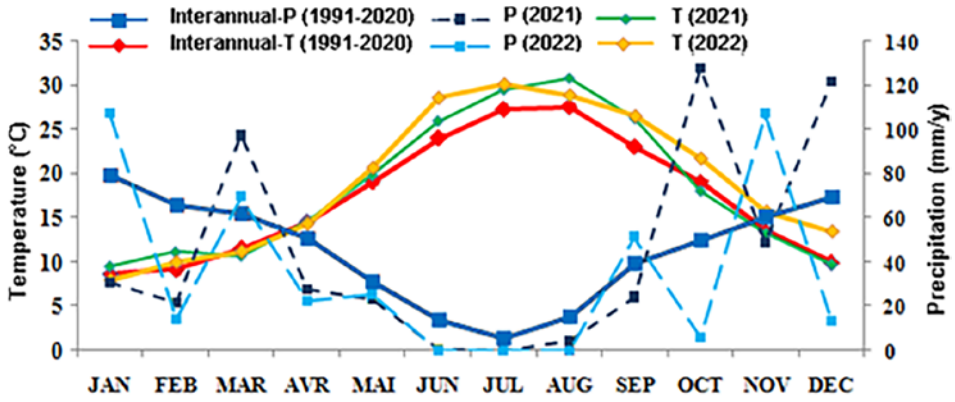

Fig. 2. Gaussen ombrothermic diagram for Sidi Smail (1991–2020).

spectively. The plain is drained by a dense hydrographic network represented by three permanent rivers: *Medjerda* river, and *Beja* and *Kasseb* wadis, and several ephemeral watercourses. The *Medjerda* river divides Sidi Smail plain into two parts: the southern part, extending from this watercourse to the hills of Djebel *Argoub El Mangouch* and of *El Matria*, and the northern part covering the area from this watercourse to the hills of Djebel *Jebil* and *Sidi Gassem*. Sidi Smail plain is among the most substantial agricultural areas in northwestern Tunisia with almost 80% of its overall area is exploited for agriculture. The fertility of soil and the availability of adequate water resources has supported the cultivation of cereals, fodder crops, olive trees, legumes, and vegetables in the plain, occupying approximately 65%, 15%, 10%, 7%, and 3% of the cultivated area, respectively (Atlas Gouvernorat de Béja, 2016). Two main types of fertilizers are commonly used in the plain to enhance the crop growth and yield: ammonium nitrate as a nitrogen-based fertilizer and diammonium phosphate (DAP N-P 20-3) as a phosphorus-based fertilizer. The recommended fertiliza-

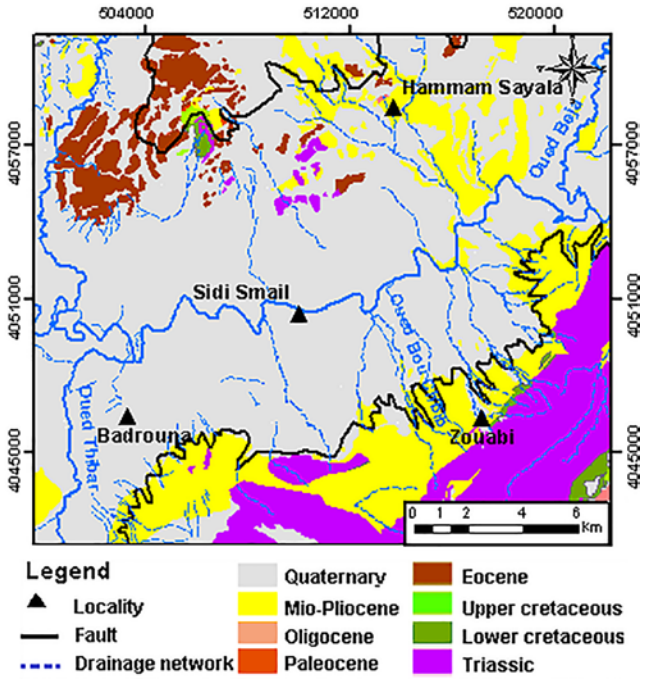

Fig. 3. Geological map of the study area.

tion rates are 250 kg/ha/year of diammonium phosphate and 550 kg/ha/year of ammonium nitrate (Ayed-Khaled *et al.*, 2017). However, most farmers apply fertilizer quantities that exceed these rates mostly during the prolonged dry periods. Based on the official crop calendars, ammonium nitrate is often applied in three splits: 1st January, 1st February and 1st March (corresponding to the beginning of the growing season and as top-dressing), whereas diammonium phosphate (DAP N-P 20-3) fertilizers are applied once at the planting stage (November-October). These timings may influence directly nitrogen availability and its transformations in soils, contributing to increased nitrate concentrations, particularly in wet periods.

According to the National Sanitation Office (ONAS) of Béja, Tunisia, the sanitary sewer network is only partially developed in Sidi Smail plain, and household wastewater is predominantly discharged into individual septic tanks. As a result, wastewater management remains limited, and treated effluents are not reused for irrigation. Leakage from septic tanks and uncontrolled infiltration of domestic wastewater may locally increase groundwater salinity and nitrate concentrations.

Sidi Smail plain corresponds to a Quaternary depression limited by the Diapiric zone and the Nappe zone to the south and north, respectively (Hamed *et al.*, 2017). The sedimentary series of the Cenozoic and Mesozoic strata underline its stratigraphy (Moussaoui *et al.*, 2023). The Mesozoic series comprise a Triassic salt deposits outcrop in Djebel *Matria*, *Touila*, *Lengua*, and *Guerouaou* (Fig. 3). These deposits, originating likely from diapiric structure, consist of evaporate and carbonate minerals (Hamed *et al.*, 2017). Most geological structures existing in the southern part of the plain comprise discontinuous sections of dolostones, sands, and clays. Marl, limestone, and sandstone of the Valanginian and Barremian–Aptian strata are the main sediments of the lower cretaceous. These sediments are followed by greyish limestone and marl of the upper Cretaceous strata, which are overlain by the Turonian–Coniacian carbonates with several microfaune associations. These deposits are covered by Santonian marls and then by the Abiod formation with clear limestone beds and marls of Campanian–Maestrichtian (Moussaoui *et al.*, 2023). Marls of Paleocene, Nummulitic limestone of Eocene, and sandy formations of Oligocene compose the Cenozoic series. These strata are followed by thick Miocene marl, which contains a few shale intercalations. The upper Plio-Quaternary series represented by alluvial deposits in the

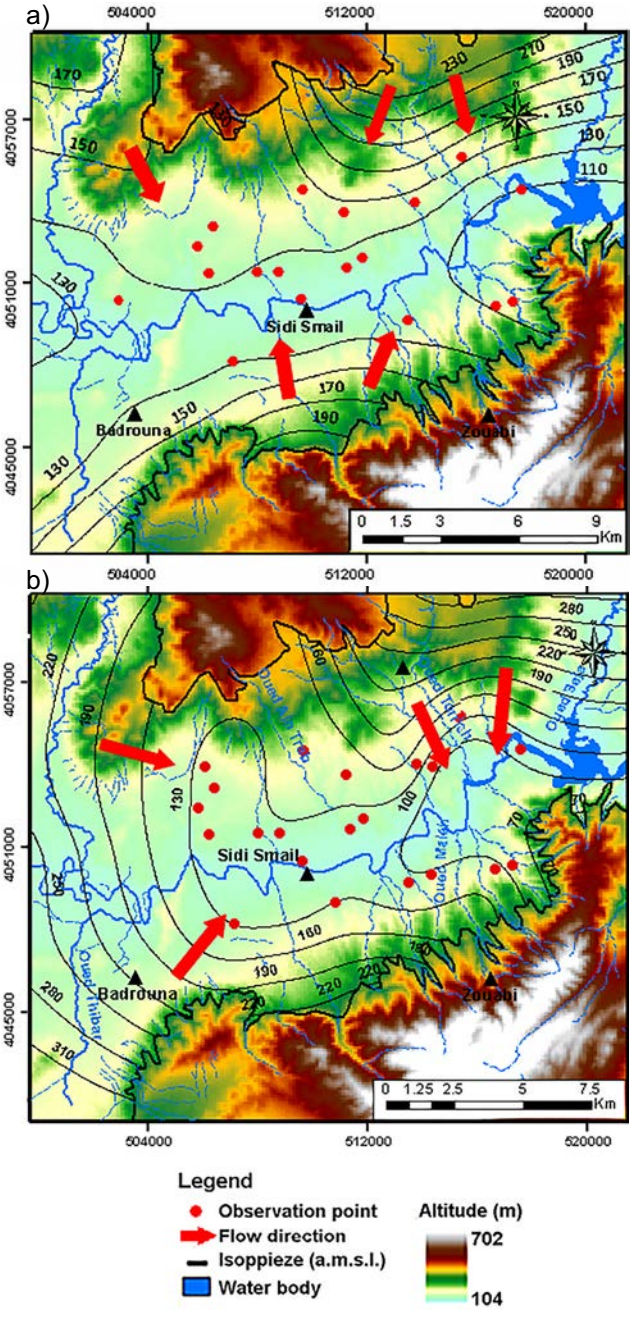

Fig. 4. Piezometric map of the (a) shallow and the (b) Pliocene aquifer of Sidi Smail (October 2021).

top and conglomeratic levels from the bottom cover a major part of the plain. Sidi Smail plain shows many faults, essentially NE-SW, NW-SE and N-S directions (Ayed-Khaled *et al*., 2017). The Triassic series provides a tectonic contact that extends through the Cretaceous as well as the Neogene strata (Fig. 3). The groundwater system in the plain comprises a multilayered aquifer formed by two principal units: a shallow Quaternary aquifer and a deeper Mio-Pliocene aquifer. These aquifers are hydraulically separated by an approximately 20-meter-thick clay layer. The Quaternary aquifer is composed of sandstones, conglomerates, and sands, and exhibits two predominant groundwater flow directions (Fig. 4a). In the northern sector of the plain, the shallow groundwater flows from northwest to southeast, whereas in the southern sector, the flow direction shifts from southwest to east, ultimately discharging into the Medjerda river and the *Sidi Salem* Dam. The Pliocene aquifer, located at depths ranging from 50 to 120 meters below ground surface, consists predominantly of gravels, sands, and clayey intercalations, forming a confined aquifer system, with groundwater flow direction from the northeastern and northwestern to the eastern part of the plain (Fig. 4b). Owing to the coarse texture of the aquifer materials and the discontinuous nature of the clay layers, vertical hydraulic connectivity between the two aquifers is likely. Accordingly, these two aquifers are considered as a single hydrological system with an average saturated thickness of approximately 80 meters. Hydraulic conductivity within the aquifer system shows spatial variability, ranging from 5.3×10^{-4} m/s in the northern and southern margins of the plain to 3.5×10^{-4} m/s in its central zone. The Quaternary aquifer is exploited by 446 wells, with a total annual abstraction of about 2.13 Mm³ in 2020 (DGRE, 2020a). The deep Pliocene aquifer is tapped by 46 boreholes, which collectively extract about 1.02 Mm³ per year (DGRE, 2020b). Both aquifers are used mainly for irrigation, while domestic water supply accounts for only a small proportion of the total abstraction (less than 5%) (DGRE, 2020b). The long-term evolution of groundwater use reveals a marked intensification of abstraction in both aquifers over the past two decades (Fig. 5). In the Quaternary aquifer, pumping volumes increased from 1.14 Mm³ in 2000 to 2.13 Mm³ in 2020, accompanied by a substantial rise in the number of wells (from 289 to 446). Abstraction from the Pliocene aquifer increased from 0.40 Mm³ in 2000 to 1.02 Mm³ in 2020, reflecting an increasing dependence on deeper groundwater resources. Historical records of piezometric levels and groundwater mineralization (TDS) in the Quaternary aquifer, measured in four monitoring wells (GW1, GW2, Well102, and Well103) collected from the Water Resources Department of the Regional Commissariat for Agricultural Development of Béja (Tunisia) show that the piezometric levels increased in these wells during the period 2001–2013, despite the continuous rise in the number of wells in the plain (Fig. 6). This rise in groundwater levels contrasts with what would normally be expected under intensified pumping. This pattern can be explained by the enhanced groundwater recharge during wetter hydrological years.

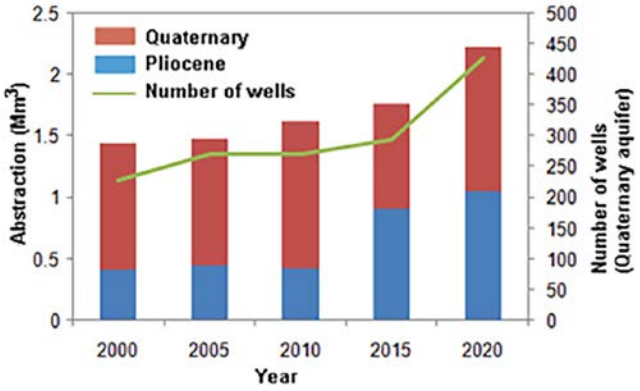

Fig. 5. Temporal variation of the groundwater abstraction and number of wells.

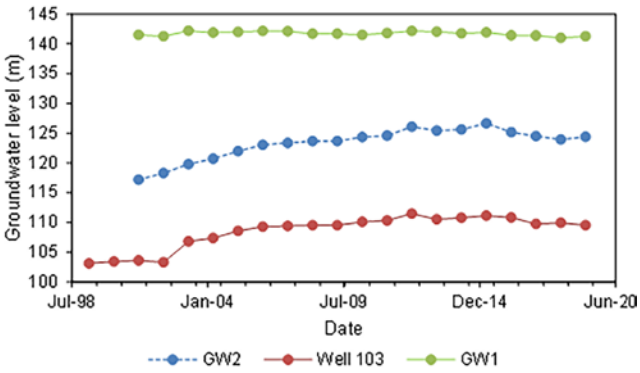

Fig. 6. Temporal evolution of the groundwater piezometric levels (Quaternary aquifer) during the period 2001–2019 in the wells GW1, GW2, and Well 103.

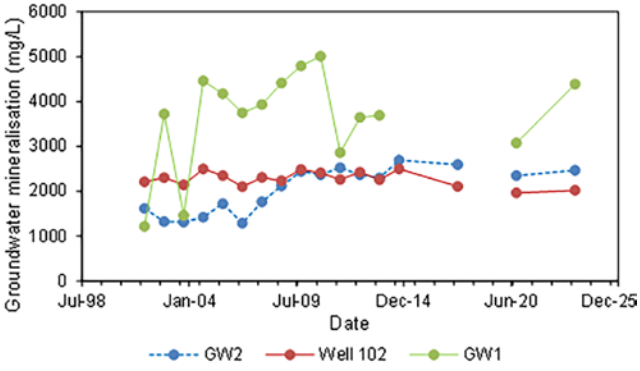

Fig. 7. Temporal variation of total dissolved solids (TDS) of the Quaternary groundwater aquifer during the period 2001–2023 in the wells GW1, GW2, and Well 102.

Piezometric levels of the shallow groundwater showed a noticeable decline between 2013 and 2019 (1.67 m in well GW2, 1.97 m in well 103, and 0.78 m in well GW1), indicating increasing stress on the aquifer system and/or decreasing groundwater recharge. Groundwater mineralization increased by 851 mg/L in the well GW2 and 3,171 mg/L in the well GW1, while it decreased by 189 mg/L in the well102 during the period 2001–2023 (Fig. 7).

MATERIAL AND METHODS

A total of 57 groundwater samples were collected in autumn (October 2021) and summer (August 2022) to assess the influence of seasonal climatic variations on groundwater quality and hydrochemistry. August corresponds to the core of the dry summer season, when temperatures and evaporative demand reach their maximum and agricultural pumping may be at its peak. In contrast, October represents autumn, which is the transitioning season toward the cooler and wetter winter season, characterized by decreasing temperatures, the first effective rainfall events, and the cessation of irrigation. Although October does not represent the fully developed wet season, long-term climatic trends (2001–2019) indicated that it is consistently distinct from the summer dry period in terms of temperature, rainfall, and hydrological conditions. Therefore, the two sampling periods capture significantly different seasonal states, allowing for an effective assessment of the influence of climatic variations on groundwater quality and hydrochemistry. The study period (October 2021 and August 2022) is representative of the multi-year period in terms of temperature and precipitation. Groundwater samples were taken from monitoring wells capturing the shallow Quaternary aquifer (well depths: 6–50 m, and groundwater-table depth: 2–23 m below the ground level) and from boreholes in the deep Pliocene aquifer (at depths: 50–125 m, and static levels at 21–49 m below the ground level). Besides, four water samples were collected from the *Medjerda* river (SW1) and its tributary the *Torch* (SW2) in order to capture their hydraulic connection with the groundwater aquifer system. Portable meter (pH/mV meter-HI8424, WTW Cond 3310) was used in *situ* to determine the water samples pH and the electrical conductivity (EC). The water samples were stored in 1L-capacity polyethylene bottles, which were already cleaned twice with distilled water and rinsed with the sampled water. In the laboratory, each water sample was filtered with a 0.45 µm pore filter paper and stored at 4°C until carrying out the chemical analysis. The total dissolved solid (TDS) of water samples was determined using the gravimetric method (APHA, 1992). The concentrations of Mg^{2+}, Na^{+}, Ca^{2+}, K^{+}, Cl^{-}, SO_4^{2-}, NO_3^{-}, NO_2^{-}, and NH_4^{+} were measured using Metrohm chromatography technique. The concentration of bicarbonate (HCO_3^{-}) was determined by volumetric titration 0.1 M using nitric acid H_2SO_4. Table 1 presents the statistical summaries of the physicochemical properties of groundwater in Sidi Smail plain. Piper, geochemical plots, correlation matrix and saturation index (SI) were used to explore the groundwater chemistry and investigate the groundwater mineralization mechanisms. The PHREEQC (version 2) code was used to calculate the saturation index (Parkhurst and Appelo, 1999). The Water quality index (WQI) model and the USSL and Wilcox diagrams were used to assess the groundwater suitability for drinking and irrigation purposes.

The water quality index (WQI) was selected in this study to evaluate the groundwater quality in Sidi Smail plain considering the relative implication of different physicochemical parameters (TDS, Cl^{-}, SO_4^{2-}, HCO_3^{-}, F^{-}, etc.) on the groundwater geochemistry. The WQI of groundwater in the autumn transition and the dry summer seasons was calculated following two steps (Tyagi *et al.*, 2013). In the first step, a weight (w) was attributed to each selected physicochemical parameter between 1 and 5, based on its influence on the groundwater quality (Table 2). Then, the relative weight (WR) was calculated as follows:

$$WR = \frac{c_w}{\sum c_w} \qquad (1)$$

The second step corresponds to the calculation of a quality characterization index (Qi) by dividing the measured concentration (Ci) of each chemical parameter by its

Table 1. Statistical summary of hydrochemical parameters of the groundwater and surface water samples. Abbreviations: BDL: below the detection limits, SD: standard deviation.

	Units	Groundwater October 2021 (n = 28)				Surface water (October 2021)		Groundwater August 2022 (n = 29)				Surface water (August 2022)	
		Min	Max	Mean	S.D	S1	S2	Min	Max	Mean	S.D	S1	S2
T	°C	19.3	26.5	22. 8	1.92	23.5	21.3	–	–	–	–	–	–
pH	–	6.3	7.8	7.1	0.33	6.6	7.4	7.11	7.63	7.36	0.11	7.54	7.62
EC	µS/cm	853	6,920	2,985	1,624	4,290	831	1,066	7,700	3,194	1,446	4,390	874
TDS	mg/L	640	5,157	2,224	1,210	2,695	646	775	5,698	2,381	1,070	3,105	920
HCO_3^{-}	mg/L	121.9	347.7	270.2	49.5	292	303	236	354	288	30.49	253	276
Cl^{-}	mg/L	105.8	1,697	560.1	379.1	954	92.4	135	2,249	677	451	981	89
SO_4^{-}	mg/L	35.29	1,460	282.2	296.6	577.1	35	49	1,200	309	254	649	55
NO_2^{-}	mg/L	BDL	13.38	2.4	3.73	0	0	–	–	–	–	0	0
NO_3^{-}	mg/L	3.54	396.1	95.3	73.8	31.2	35.4	6.6	357	87.41	66.94	26.8	53.6
F^{-}	mg/L	0.3	1.9	0.8	0.49	0.57	0	0.56	3.06	1.37	0.62	2.25	0.45
Br^{-}	mg/L	BDL	3	0.9	0.76	1.1	0	BDL	3.31	1.62	0.77	0	0.56
Ca_2^{+}	mg/L	83.0	581.4	216.4	106.9	213	109.4	23	525	236	101	192	110
Mg_2^{+}	mg/L	14.1	176.9	55.4	34.8	31.9	11.9	15	245	65.24	45.43	72	13
Na^{+}	mg/L	72.5	1,079	267.91	217	579.2	57.2	97	733	288	156	726	73
K^{+}	mg/L	0.11	17.7	3.6	3.72	15.2	1.1	0.33	12.21	2.83	2.89	6.35	1.2
NH_4^{+}	mg/L	BDL	5.3	0.3	1.01	0	0	–	–	–	–	0	0

corresponding standard (C_{OMS}) according the World Health Organization limits (WHO, 2022).

$$Q_i = (\frac{c_i}{c_{OMS}}) \times 100 \quad (2)$$

Finally, the WQI was calculated by adding the SI for each physico-chemical parameter in each groundwater sample:

$$IQE = \Sigma SI \quad (3)$$

where SI was calculated as follows:

$$SI = WR \times Qi \quad (4)$$

The ArcGIS 10.3 software was used to develop the spatial distribution maps for TDS, concentrations of Na^+, Ca^{2+}, Cl^-, SO_4^{2-}, and NO_3^-, and WQI in Sidi Smail plain.

The quality of irrigation water influences the crop yield and physical properties of the soil. The sodium adsorption ratio (SAR), the sodium percentage (%Na), and the United States Salinity Laboratory (USSL) the Wilcox diagrams were used to evaluate the groundwater quality for irrigation purpose in *Sidi Smail* plain. The USSL diagram classifies the groundwater quality for irrigation using SAR and EC values. These parameters were computed using the following equations (Yildiz and Karakuş, 2020):

$$SAR = \frac{Na}{\sqrt{\frac{Ca+Mg}{2}}} \quad (5)$$

$$\%Na = \frac{Na+K}{Ca+Mg+Na+K} \times 100 \quad (6)$$

where all the concentrations are expressed in meq/L

RESULTS AND DISCUSSION

pH of groundwater

The groundwater pH in Sidi Smail plain ranged from 6.26 to 7.83 in autumn 2021 (average: 7.05) and from 7.11 to 7.63 in summer 2022 (average: 7.36), indicating a slightly acidic to slightly alkaline character in the autumn and slightly alkaline in the summer. In both seasons, the pH values mostly fell within the acceptable range for drinking water (6.5–8.5), as recommended by the WHO (2022), except in the autumn for two wells (GW10 and GW19) and two boreholes (GW13 and GW15). The slightly acidic conditions observed during this season in wells GW10 and GW19 may be attributed to rainwater infiltration, which reacts with CO_2 from root respiration and organic matter decomposition to form weak carbonic acid (Liu *et al*., 2025). This process increases the H^+ concentration, thereby lowering pH. Additionally, the excessive use of fertilizers in agricultural activities may contribute to acidification in these wells. In the deeper Mio-Pliocene aquifer, the slightly acidic pH in boreholes GW13 and GW15 is likely due to the presence of sandy gravel deposits with low buffering capacity. In certain zones lacking carbonate minerals, inorganic acidification can occur (Serrano *et al*., 2016). Conversely, about 86% of groundwater samples (n = 24) exhibited in the autumn slightly alkaline conditions, primarily due to the presence of CO_3^{2-} and HCO_3^- ions. This alkalinity can be explained by carbonate dissolution processes and potentially high concentrations of major ions.

Table 2. Relative weight of physico-chemical parameters used to compute the WQI.

Parameter	C_{OMS}	Cw	WR
Salinity	1,000	5	0.15
Chlorides	200	3	0.1
Sulfates	250	2	0.06
Bicarbonates	250	1	0.03
Fluorides	1.5	5	1.15
Calcium	200	3	0.1
Magnesium	150	3	0.1
Sodium	200	3	0.1
Potassium	30	3	0.1
Nitrates	50	5	1.15
		Total Cw = 33	Σ WR = 1

Groundwater electrical conductivity and mineralization

The groundwater electrical conductivity (EC) indicated substantial spatiotemporal variability in Sidi Smail plain, ranging from 853 to 6,920 µS/cm in the autumn (average: 2,985 µS/cm; n = 28) and from 1,066 to 7,700 µS/cm in the summer (average: 3,194 µS/cm; n = 29). The lower range of groundwater EC values recorded in the autumn can be attributed to the repeated irrigation during the hot and dry summer season to compensate the large evaporative demand. The percolation of excess irrigation water may dilute the groundwater and thus decrease its mineralization and salinity (EC). Groundwater mineralization in Sidi Smail plain varied from 640 to 5,157 mg/L in the autumn (average: 2,225 mg/L; n = 28), and from 775 to 5,698 mg/L in the summer (average of 2,381 mg/L; n = 29). These TDS average values exceed the mineralization of the water samples collected from the Torch wadi in the autumn (TDS = 646 mg/L) and the summer (TDS= 920 mg/L) but they were lower than the TDS values of water samples taken from the *Medjerda* river in the autumn (TDS = 2,695 mg/L) and the summer (3,105 mg/L). The Medjerda River mainly functions as a drainage channel, but local conditions allow partial infiltration into the aquifer. This contributes to slightly increased groundwater mineralization near the river, while the likely infiltration of fresh water from the Torch wadi dilutes groundwater in the northern sector, lowering EC and TDS values (Fig. 6a, b).

The results indicated that the surface and groundwater mineralization increased in the summer as consequence of the increase in the evaporative demand. The spatial distribution of the groundwater mineralization shows that the minimum TDS values during the autumn and the summer seasons were observed in the northern sector of the plain. The rainfall recharge and the fresh water seepage through faults intersecting the Ypresian karstic formations located

in this sector play a key role in the groundwater dilution. These fault systems may serve as preferential flow pathways, enhancing recharge and groundwater movement. The highest groundwater TDS values in the autumn were measured in southern sector of the plain at the foothills of Djebel Argoub El Mangouch. These results are attributed to the dissolution of Triassic evaporites deposits, corroborating findings by Ayadi *et al.* (2018), who reported large mineralization of groundwater near Triassic outcrops in the Teboursouk region in northwestern Tunisia. Additional, high mineralization levels were observed in the wells GW20 and GW25, which are located in the central sector of the plain, likely due to salt leaching from soils exacerbated by irrigation with saline water and intense rainfall events. The wells GW2 and GW9, which are situated near the Medjerda river, were particularly vulnerable to brackish and saline water intrusion from the riverbed. Based on the WHO guideline value of 1,000 mg/L for drinking water (WHO, 2022), groundwater from about 89% of monitoring wells and boreholes in the autumn (n = 25) and 93% of monitored wells and boreholes in the summer (n = 27) is unsuitable for human consumption due to excessive mineralization. Fresh water samples (TDS < 1,000 mg/L) were identified in three monitoring wells and boreholes in the autumn and only two monitoring wells and boreholes in the summer.

Concentrations of Na^+ and Cl^-

The chloride and the sodium are the major ions in the groundwater in the autumn and the summer seasons. The concentration of Na^+ varied from 72.5 to 1,079 mg/L in the autumn (average: 268 mg/L) and from 97 to 733 mg/L in the summer (average: 288 mg/L). Sodium content in about 53% of groundwater samples (n = 15) in the autumn and in 62% of groundwater samples (62%, n = 18) in the summer are above the threshold limit value of 200 mg/L (WHO, 2022). This cation in the groundwater can arise from dissolution of Triassic evaporites deposits as well as ion exchange reactions. Chloride concentration ranged from 106 to 1,697 mg/L in the autumn (average: 560 mg/L) and from 135 to 2,249 mg/L in the summer (average: 677 mg/L). The concentration of Cl^- exceeds the WHO (2022) threshold limit of 250 mg/L in about 82% groundwater samples (n =23) in the autumn and 89% groundwater samples (n =26) in the summer. The occurrence of this anion in the groundwater could result from the dissolution of Triassic evaporites, the use of chemical fertilizers and livestock manure in agriculture, and the return flow from irrigation. The average concentrations of Na^+ and Cl^- ions showed slight increase in summer, likely due to return flow from irrigation, which enhance the halite dissolution in the unsaturated zone of soil. The Na^+ versus Cl^- scatter plot reveals that about 28% of groundwater samples (n =8) in the autumn and 17% of groundwater samples (n = 5) in the summer align closely with the 1:1 bisector line, suggesting that the dissolution of halite minerals is a dominant source of these ions (Fig. 7a). In contrast, about 72% of groundwater samples (n =20) in the autumn and 86% of groundwater samples (n = 25) in summer exhibit an excess of chloride, which may be attributed to anthropogenic inputs. These include the application of potassium chloride (KCl) fertilizers in agriculture, chloride leaching from livestock manure, and likely infiltration from septic tanks (Katz *et al.*, 2011). Chloride shows strong positive correlations with TDS in autumn and summer seasons indicating that the groundwater mineralization is influenced by this anion (Fig. 7b).

Concentrations of Ca^{2+}, Mg^{2+}, SO_4^{2-} and HCO_3^-

The concentration of Ca^{2+} varied from 83 to 581 mg/L in the autumn (average: 216 mg/L) and from 23 to 525 mg/L in the summer (average: 236 mg/L). Calcium content in about 46% of groundwater samples (n =13) in the autumn and 58% of groundwater samples (n =17) in the summer are above the threshold limit value of 200 mg/L (WHO, 2022). This cation in the groundwater can arise from dissolution of Triassic evaporites deposits as well as ion exchange reactions (Askri *et al.*, 2022. The concentration of SO_4^{2-} varied from 35 to 1,460 mg/L in the autumn (average: 282 mg/L) with 46% of groundwater samples (n =13) had concentration above the threshold limit of 200 mg/L (WHO), and varied from 49 to 1,200 mg/L in the summer (average: 309 mg/L) with about 55% of groundwater samples (n = 16) had

Table 3. Pearson correlation matrix of the groundwater samples (wet season).

	pH	TDS	EC	Ca^{2+}	Mg^{2+}	K^+	Na^+	Cl^-	SO_4^{2-}	HCO_3^-	NO_3^-	F^-	Br^-
pH	1												
TDS	0.217	1											
EC	0.191	**0.833**	1										
Ca^{2+}	0.298	0.518	**0.635**	1									
Mg^{2+}	0.346	0.476	0.581	**0.941**	1								
K^+	-0.020	0.593	**0.632**	0.286	0.281	1							
Na^+	0.042	**0.720**	**0.850**	0.319	0.317	**0.827**	1						
Cl^-	0.152	**0.715**	**0.939**	0.575	0.556	**0.739**	**0.919**	1					
SO_4^{2-}	0.219	0.497	0.424	**0.758**	**0.773**	0.434	0.340	0.370	1				
HCO_3^-	0.348	0.354	0.312	0.178	0.181	0.161	0.319	0.309	0.085	1			
NO_3^-	-0.029	0.297	0.425	0.297	0.250	-0.191	0.169	0.335	-0.182	0.031	1		
F^-	0.207	0.535	**0.606**	0.251	0.353	0.451	**0.672**	**0.622**	0.241	0.428	0.308	1	
Br^-	0.038	-0.057	0.208	0.286	0.195	0.014	0.092	0.301	-0.191	0.251	0.412	0.080	1

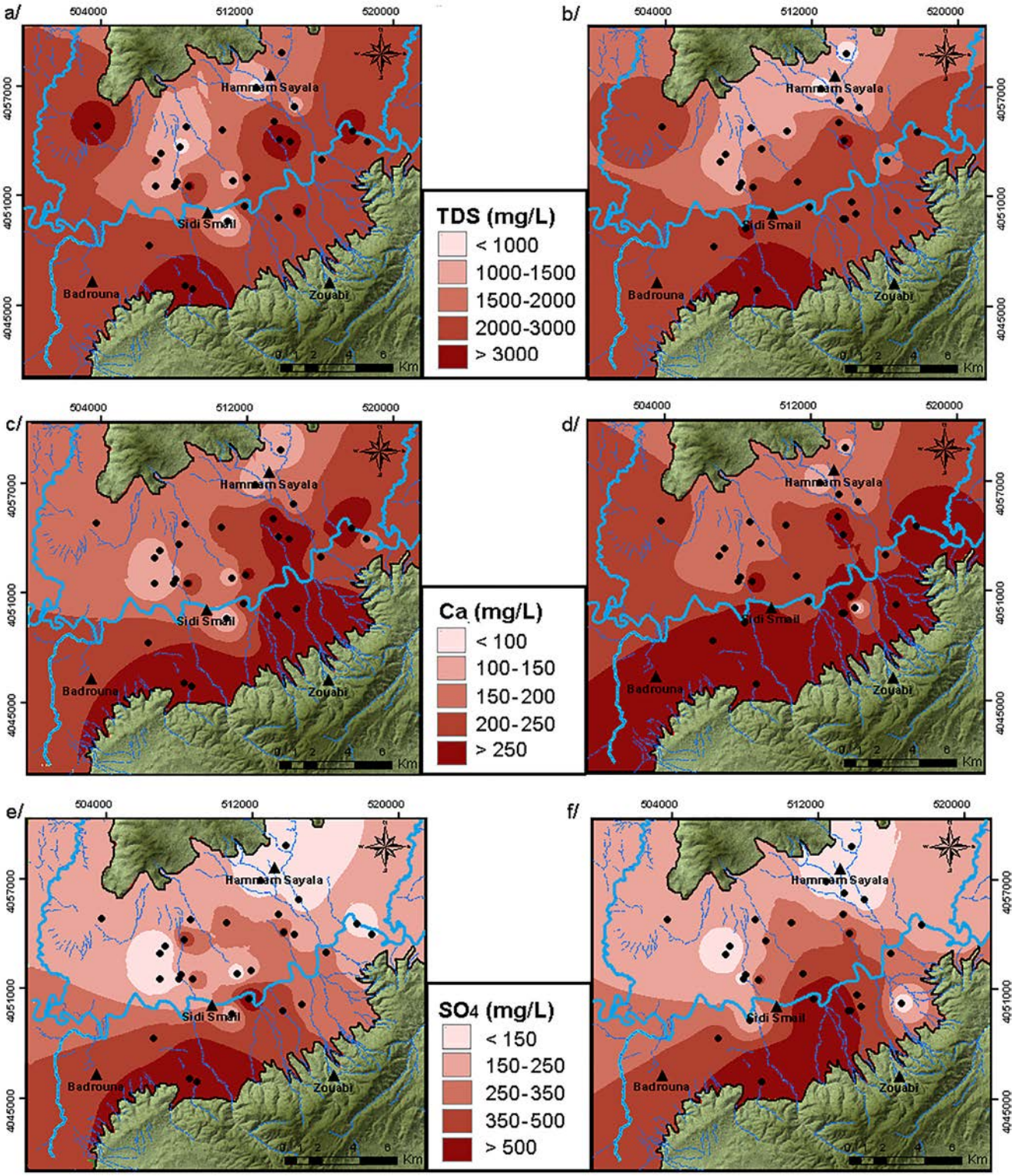

Fig. 8. a) Spatial distribution map of TDS (wet season); (b) dry season; (c) Spatial distribution map of Calcium (wet season); (d) dry season; (e) Spatial distribution map of sulfates (wet season); (f) dry season.

concentration above this limit. The concentration of Ca^{2+} and SO_4^{2-} decreased in both seasons from the south to the north of the plain in the flow direction (Fig. 8c–f). About 18% of groundwater samples (n = 5) in the autumn fall along the bisector line in the Ca^{2+} vs. SO_4^{2-} scatter diagram, suggesting that these ions are derived from dissolution of gypsum and anhydrite (Fig. 9c). About 79% of groundwater samples (n = 22) are placed above the bisector line, indicating excess of Ca^{2+} likely due to reverse ionic exchange and/or silicate dissolution processes. A single groundwater sample in the autumn falls below the bisector line highlighting Ca^{2+} depletion likely due to ionic exchange

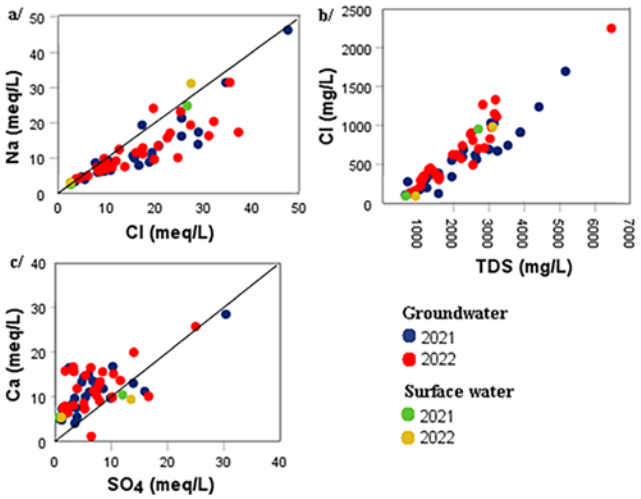

Fig. 9. (a) Na^+ vs. Cl^-; (b) Ca^{2+} vs. SO_4^{2-} and (c) Cl^- vs. TDS.

between the groundwater and the matrix of clay mineral (Alzahrani *et al.*, 2025). The concentration of Mg^{2+} varied from 14 to 177 mg/L in the autumn (average: 55 mg/L) and from 15 to 245 mg/L in the summer (average: 62.24 mg/L). The highest concentrations of this cation were observed in the last season. Magnesium in the groundwater may originate from the dissolution of magnesium-bearing minerals such as magnesite ($MgCO_3$) and certain clay minerals, as well as from the application of magnesium-containing fertilizers. The strong correlations observed between Ca^{2+} and Mg^{2+} (r = 0.94) in the autumn and (r = 0.57) in the summer suggest that these ions are predominantly derived from the dissolution of rock-forming minerals such as dolomite and magnesium calcite (Tables 3 and 4). Additionally, the significant correlation between Mg^{2+} and SO_4^{2-} (r = 0.77) in the autumn and (r = 0.64) in the summer indicates a common geochemical origin, likely associated with the dissolution of dolomite and other magnesium-bearing minerals.

The concentration of HCO_3^- varied from 122 to 348 mg/L in the autumn (average: 270 mg/L) and from 236 to 354 mg/L in the summer (average: 288 mg/L). The weak correlations between HCO_3^- and Ca^{2+} (r = 0.178), and between HCO_3^- and Mg^{2+} (r = 0.181) in the autumn suggest that these ions are primarily derived from processes other than the weathering of carbonate minerals such as calcite and dolomite (Sampath *et al.*, 2022).

The wide spatial variability observed in groundwater EC, TDS, and concentration of several major ions suggest that the hydrochemistry of the aquifer in Sidi Smail plain is governed by multiple geochemical processes, including mineral dissolution, soil salt leaching, and ion exchange reactions.

Chemical water facies

The Piper diagram (1944) indicates that the groundwater in Sidi Smail plain in the autumn and the summer seasons is classified into three hydro-chemical facies (Fig. 10):

– Mixed facies Ca-Mg-Cl,
– Na-Cl facies,
– Ca-Cl facies.

The prevalence of the mixed Ca-Mg-Cl facies may reflect the dissolution of Triassic evaporites deposits. Regarding surface waters, samples from the Medjerda river (SW1) display a Na-Cl facies, while those from the *Torch* wadi (SW2) correspond to a Ca-Mg-HCO_3 facies. The presence of the Na-Cl facies in both Medjerda river and five groundwater samples in the autumn suggests that (i) surface and groundwater may be influenced by similar hydrochemical processes, and (ii) a hydraulic connection exists between the Medjerda River and the Quaternary aquifer, indicating potential surface water-groundwater interactions (Irvine *et al.*, 2024).

Geochemical modeling

The geochemical modeling results obtained using PHREEQC (Table 5) indicated that all groundwater samples collected in the autumn exhibit undersaturation with respect to halite, gypsum, and anhydrite, indicating active dissolution of these evaporite minerals primarily from Triassic salt deposits. This process contributes significantly to the enrichment of Na^+, Cl^-, Ca^{2+}, and SO_4^{2-} ions in the groundwater, thereby increasing both electrical conduc-

Table 4. Pearson correlation matrix of the groundwater samples (dry season). Bold indicates significant correlation coefficient.

	pH	TDS	EC	Ca^{2+}	Mg^{2+}	K^+	Na^+	Cl^-	SO_4^{2-}	HCO_3^-	NO_3^-	F^-	Br^-
pH	1												
TDS	-0.044	1											
EC	-0.042	**0.949**	1										
Ca^{2+}	0.124	**0.674**	**0.725**	1									
Mg^{2+}	0.190	**0.873**	**0.859**	0.579	1								
K^+	-0.235	0.056	0.065	0.007	-0.085	1							
Na^+	-0.353	**0.699**	**0.810**	0.394	0.492	0.114	1						
Cl^-	-0.005	**0.898**	**0.941**	**0.632**	**0.780**	0.043	**0.817**	1					
SO_4^{2-}	-0.066	0.542	0.512	0.474	**0.646**	0.165	0.172	0.237	1				
HCO_3^-	-0.053	-0.059	0.027	-0.032	0.139	-0.335	0.011	-0.101	0.197	1			
NO_3^-	-0.350	0.320	0.358	0.151	-0.018	0.107	**0.697**	0.386	-0.133	-0.325	1		
F^-	-0.151	**0.861**	**0.931**	**0.609**	**0.694**	0.038	**0.912**	**0.915**	0.330	-0.025	0.571	1	
Br^-	0.328	**0.761**	**0.772**	**0.696**	**0.785**	-0.134	0.478	**0.843**	0.167	-0.095	0.122	**0.680**	1

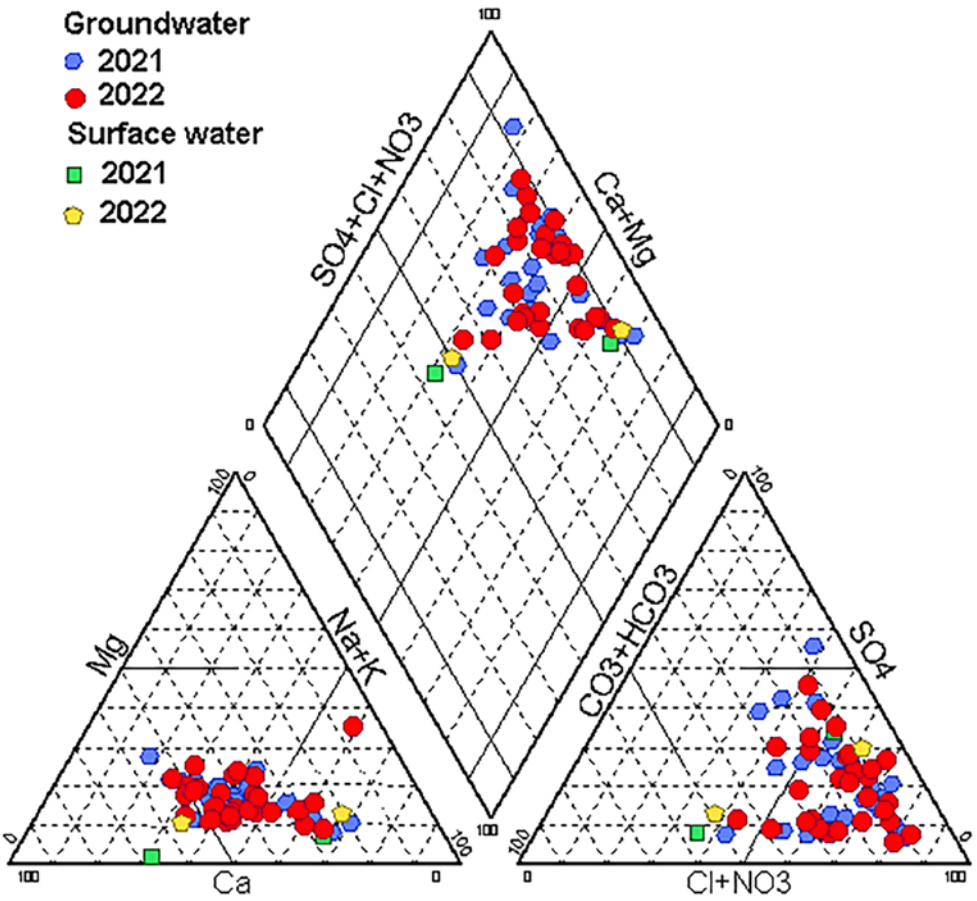

Fig. 10. Piper diagram for surface and groundwater samples.

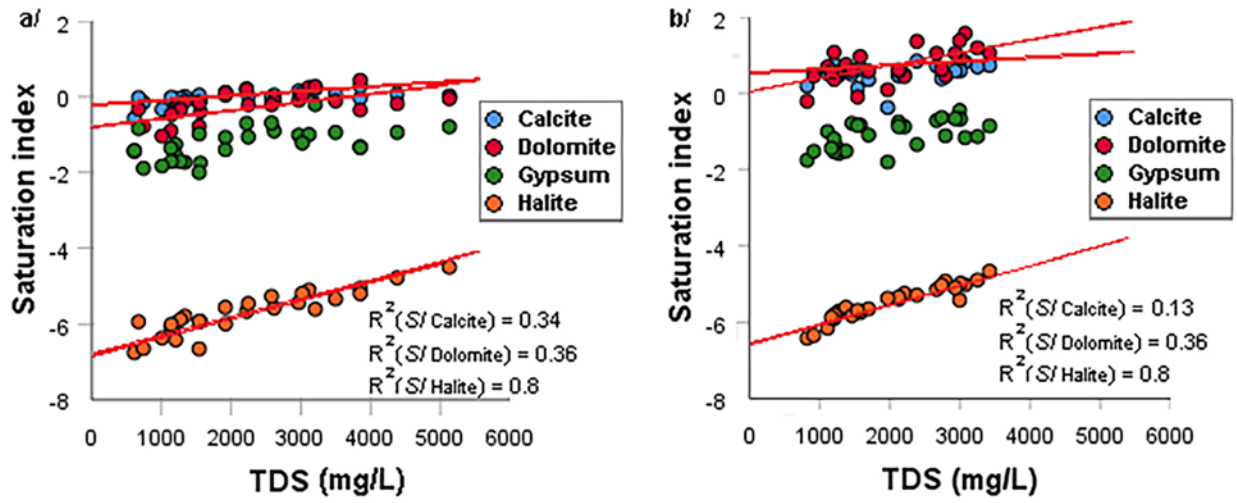

Fig. 11. Variation of SI vs. dissolved solids (TDS) in groundwater (a) wet season; (b) dry season.

tivity (EC) and total dissolved solids (TDS) concentrations (Fig. 11a, b). In terms of carbonate mineral stability, 71% of the groundwater samples collected in the autumn are supersaturated with respect to calcite, while the same proportion of samples are undersaturated with respect to dolomite. This indicates the likely precipitation of calcite and aragonite, and concurrent dissolution of dolomite. The observed slight increasing trend in the saturation indices of calcite (SI-calcite) and dolomite (SI-dolomite) with increasing TDS suggests that precipitation of these minerals may occur under more saline conditions, accompanied by a reduction in Ca^{2+} and Mg^{2+} concentrations. The preferential precipitation of calcite may lead to a depletion of Ca^{2+} in groundwater, potentially enhancing the dissolution of gyp-

Table 5. Saturation indices of the groundwater samples.

Sample No	Wet season (October 2021)					Dry season (August)				
	Anhydrite	Gypsum	Halite	Calcite	Dolomite	Anhydrite	Gypsum	Halite	Calcite	Dolomite
GW1	-1.11	-0.89	-4.72	0.13	-0.13	-1.13	-0.91	-4.71	0.68	1
GW 2	-1.12	-0.89	-5.28	0.12	-0.06	-0.99	-0.77	-5.19	0.66	1
GW 3	-1.92	-1.7	-5.87	-0.03	-0.34	-1.85	-1.63	-5.76	0.42	0.52
GW 4	-1.5	-1.27	-4.99	0.01	-0.30	-1.39	-1.17	-4.97	0.39	0.41
GW 5	-1.44	-1.21	-6.36	0.02	-0.22	-1.28	-1.06	-6.21	0.46	0.64
GW 6	-1.19	-0.96	-5.38	0.21	-0.04	-1.15	-0.93	-5.29	0.44	0.39
GW 7	-1.08	-0.85	-5.52	0.10	-0.05	-1.04	-0.81	-5.45	0.41	0.54
GW 8	-1.24	-1.02	-5.94	0.17	0.14	-1.11	-0.89	-5.80	0.59	0.91
GW 9	-1.48	-1.29	-5.14	0.33	0.49	-1.39	-1.22	-5.07	0.77	1.52
GW 10	-0.96	-0.74	-4.44	0.08	0					
GW 11	-1.71	-1.49	-5.92	-0.03	-0.32	-1.68	-1.46	-5.84	0.43	0.45
GW 12	-1.5	-1.31	-6.02	-0.37	-0.85	-1.48	-1.25	-5.96	0.70	1.02
GW 13	-1.87	-1.68	-5.73	0.06	-0.07					
GW 14	-1.88	-1.66	-5.82	0.02	-0.29	-1.79	-1.57	-5.66	0.52	0.70
GW 15	-1.15	-0.93	-5.87	0.10	-0.11	-1.07	-0.84	-5.88	0.44	0.54
GW 16	-1.89	-1.66	-5.95	0.04	-0.42	-1.81	-1.59	-5.85	0.38	0.31
GW 17	-2.02	-1.78	-6.31	-0.28	-0.99	-1.13	-0.93	-5.39	0.40	0.56
GW 18	-1.61	-1.37	-6.7	-0.52	-1.39					
GW 19	-0.87	-0.64	-5.21	0.03	-0.16	-0.91	-0.69	-5.08	0.33	0.58
GW 20	-1.18	-0.95	-5.04	0.23	0.30	-1.13		-4.94	0.62	1.08
GW 21	-0.37	-0.15	-5.55	0.26	0.32	-0.53	-0.30		0.38	0.75
GW 22	-0.88	-0.65	-5.61	0.26	0.24	-0.73	-0.51	-5.47	0.79	1.33
GW 23	-1.58	-1.35	-5.5	0.09	0.15					
GW 24	-1.25	-1.01	-5.4	0.07	-0.16					
GW 25	-1.4	-1.17	-5.13	0.16	0.09	-1.42	-1.19	-4.94	0.64	1.14
GW 26	-2.06	-1.84	-6.59	-0.10	-0.73	-2.04	-1.81	-6.47	0.14	-0.26
GW 27	-1.02	-0.79	-5.88	0.03	-0.27					
GW 28	-2.18	-1.95	-6.6	-0.08	-0.73	-1.80	-1.58	-6.40	0.44	0.40
GW 29						-1.72	-1.50	-5.93	0.48	0.52
GW 30						-1.62	-1.40	-5.34	0.79	1.31
GW 31						-0.95	-0.73	-5.03	0.54	0.88
GW 32						-2.08	-1.86	-5.42	-0.43	0.04
GW 33						-0.94	-0.72	-5.15	0.53	1
GW 34						-1.37	-1.15	-5.70	0.30	0.53
GW 35						-1.13	-0.90	-5.74	0.07	-0.15

sum and dolomite to reestablish ionic balance, particularly for calcium (Rajmohan *et al.*, 2022). Similar geochemical processes have been documented in several studies conducted in northern Tunisia (Slimani *et al.*, 2024).

Concentrations of NO_3^-, NO_2^- and NH_4^+

Nitrate (NO_3^-) concentrations in the groundwater samples collected in Sidi Smail plain ranged widely from 3.5 to 396.1 mg/L in the autumn (average: 95 mg/L) and from 6.6 to 357 mg/L in the summer (average: 87.41 mg/L). About 75% of groundwater samples (n =21) in the first season and 75% of groundwater samples (n = 22) in the second one exceeded the World Health Organization (WHO, 2022) guideline value of 50 mg/L for nitrate, level that may pose potential health risks to both humans and livestock. These results indicated that the groundwater in Sidi Smail plain is severally contaminated by nitrates. The highest nitrate concentrations are observed in the northeastern and northwestern sectors of the plain, likely due to the intensive application of nitrate-based fertilizers and/or leakage from aging septic tanks (Fig. 12a, b). These two sectors correspond to the major agricultural lands, where the use of di-ammonium phosphate (DAP N-P 203) and ammonium nitrate fertilizers and of livestock manure may increase the nitrate concentration and alter the groundwater quality. Furthermore, the high nitrate concentrations recorded in October 2021 may be related to the timing of the fertilization, particularly the DAP N-P 203 application, which is carried out in October-November. The soil fertilization during this period increases nitrogen availability in soils, whereas rainfall and repeated irrigation facilitate its dissolution and leaching into the shallow aquifers. In addition, the widespread use of poorly maintained septic tanks in the region may further contribute to elevated nitrate levels. The high coefficient of variation for nitrate calculated as the ratio of standard deviation to the mean (0.78 during the season and 0.75 during

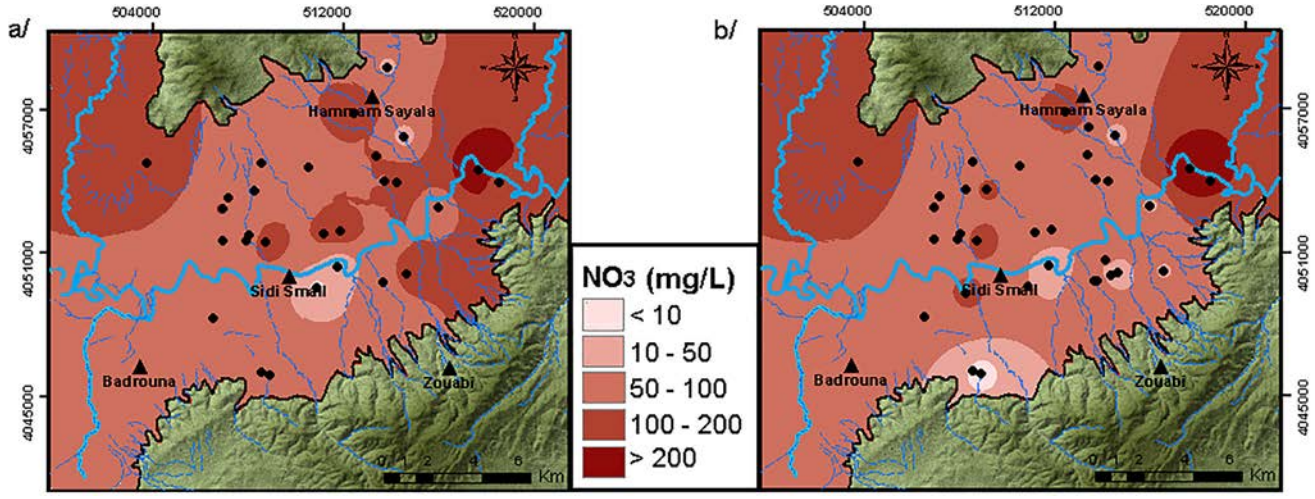

Fig. 12. Spatial distribution of nitrates concentration (a) wet season; (b) dry season.

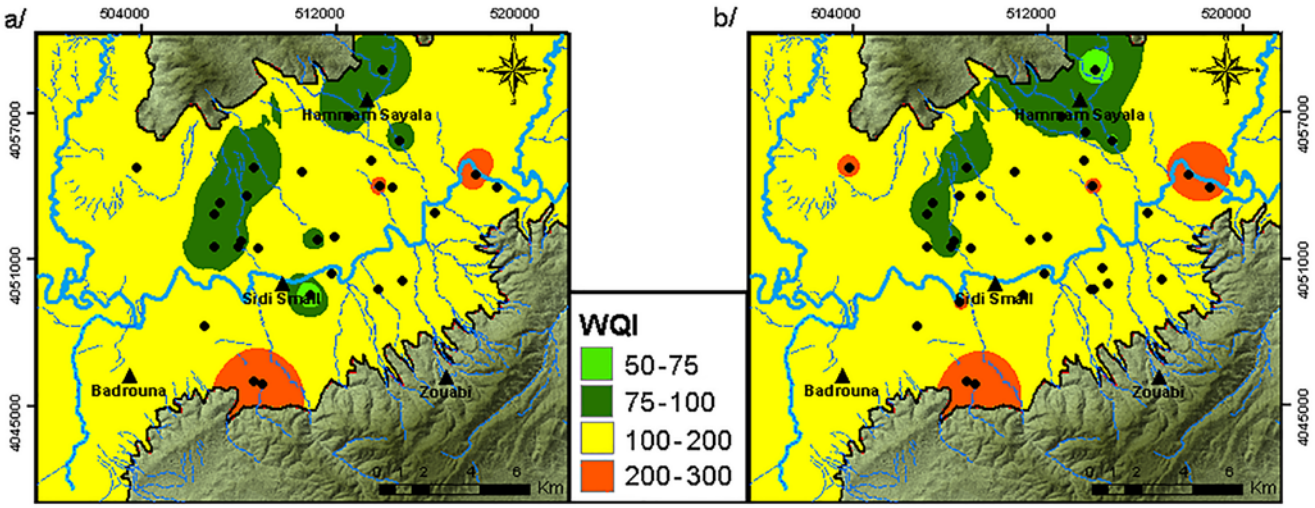

Fig. 13. Spatial distribution of WQI in the study area (a) wet season and (b) dry season.

the dry season), highlights the strong spatial variability of nitrate concentration across the plain. This variability can be attributed not only to differences in nitrate fertilizer application rates but also to other factors such as water table depth, cropping systems, soil texture, and groundwater recharge rates (Askri *et al*., 2022). The interaction of these environmental parameters generates complex spatial patterns of nitrate contamination. Additionally, the geological heterogeneity of the unsaturated zone influences the vertical and lateral movement of nitrates. Although NO_3^- levels were generally high across the plain of Sidi Smail, ammonium (NH_4^+) and nitrite (NO_2^-) were not detected in any of the sampled wells during the wet and dry seasons and were only observed in two boreholes (GW11 and GW12), both located in the northern part of the plain. This pattern suggests that nitrate is transported from the plant root zone to the groundwater through the unsaturated soil profile with minimal biological transformation. The absence of significant denitrification likely reflects a high-oxygen environment and/or a deficiency in organic carbon, which is essential as a reducing agent in the denitrification process. Tlili-Zrelli *et al*. (2018) explained the absence of ammonium and nitrite by the well-oxygenated groundwater.

Groundwater quality for drinking and irrigation uses

The water quality index (WQI) varied from 45 to 284 in the autumn (average 135) and from 63 to 271 in the summer (average 139). These results indicated that the groundwater quality was slightly deteriorated in the last season, likely due the increase of the concentration of most major ions. According to the WQI values reported in Table 6, the groundwater samples collected in the autumn are classified as of excellent quality (3%), good quality (36%), poor quality (47%), and very poor quality (14%). In the summer, the groundwater was classified as good quality (37%), poor quality (43%), and very poor quality (20%). These results indicated that the percentage of poor quality, while the very poor quality increased in summer. The spatial distribution of the water quality index shows that the highest WQI values are found in the middle and the northwestern sectors of the plain, which corresponds to the recharge areas, due

Table 6. Classification of groundwater quality for drinking and irrigation purposes.

Parameter	Range	Water quality	No. of groundwater samples	
			October 2021	August 2022
WQI	>50	excellent	3%	–
	50–100	good	36%	38%
	100–200	poor	47%	41%
	200–300	very poor	14%	21%
SAR	<10	excellent	92%	94%
	10–18	good to doubtful	8%	6%
	18–26	unsuitable	–	–
%Na	>75	excellent	–	–
	25–75	good	96%	96%
	<25	unsuitable	4%	4%

Table 7. Statistical summary of water quality parameters in both seasons.

Parameter	Wet season (October 2021)			Dry season (August 2022)		
	Min	Max	Mean	Min	Max	Mean
SAR	1.71	14.92	4.16	1.19	10.04	4.06
%Na	17.32	70.52	41.07	24.16	63.46	41.03

to the presence of highly permeable deposits (Medjerda alluvium and karstic formation) (Fig. 13a, b). The statistical summary of the selected parameters for irrigation water quality are presented (Table 7). The sodium adsorption ratio (SAR) in the groundwater samples ranged from 1.71 to 14.92 in the autumn (average: 4.16) and from 1.91 to 10.04 in the summer (average: 4.06). The USSL diagram shows that almost all the groundwater samples fall into the C3-S1 category during both seasons with low sodium adsorption ratio and high salinity. In the southern sector of the plain, characterized by a high EC values, the groundwater samples fall into C4-S2 to C4-S4 categories, with high salinity and low-to-medium SAR values (Fig. 14). Therefore, these waters can be used only for irrigation of salt-tolerant crops, which limits their suitability for irrigation. The Na value of groundwater samples varied from 17.32% to 70.52% in the autumn (average 41.07) and from 24.16% to 63.46% in summer (average 41.03). The Wilcox diagram indicates that the majority of the groundwater samples in both seasons are classified as doubtful to unsuitable (Fig. 15).

CONCLUSIONS

Seasonal and spatial variations of groundwater quality in the agricultural plain of *Sidi Smail*, northwestern Tunisia, were investigated using data of physicochemical characteristics collected in the autumn (October 2021) and the summer (August 2022). The suitability of groundwater for drinking purpose was evaluated using the Water Quality Index (WQI), while for irrigation use was studied using the SAR and %Na. Electrical conductivity (EC), total dissolved solids (TDS), along with concentrations major ions displayed temporal and spatial variations, with elevated levels observed in the southern sector of the plain during the dry summer season. Anthropogenic pressures, including limited wastewater management, intensive groundwater abstraction, overuse of fertilizers in agriculture, combined with geogenic processes and climatic factors, likely drive the observed variations in groundwater quality. The dissolution of Triassic evaporite and carbonate deposits exposed in the foothills of Djebel Argoub, El Mangouch and El Matria and the likely local infiltration of saline water from the Medjerda River into the aquifer system increased the groundwater mineralization in the southern and the central sectors of the plain, respectively. The groundwater recharge through fault systems intersecting the Ypresian karst formations decreased its mineralization in the northern sector of the plain. The hydrochemical facies, identified through the Piper diagram, reveal three main water types: mixed Ca-Mg-Cl, Na-Cl, and Ca-Cl. About 71% and 75% of the groundwater samples exhibited during the autumn and the summer seasons, respectively, concentrations of

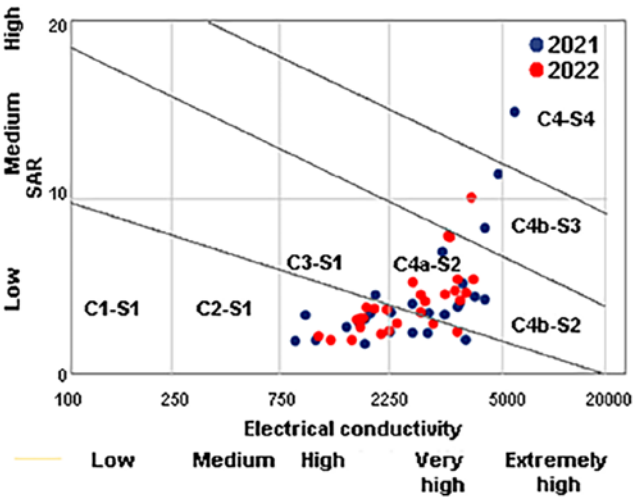

Fig. 14. USSL diagram of the groundwater samples in the different seasons.

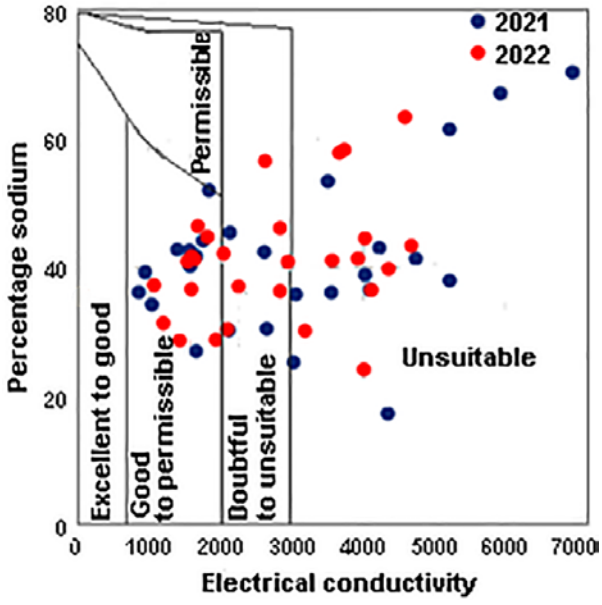

Fig. 15. WILCOX diagram of the groundwater samples in the study area.

nitrate above the World Health Organization (WHO, 2022) guideline value of 50 mg/L. This may pose a substantial public health risk. The water quality index indicates that most groundwater samples (>50%) in the plain present poor-to-very poor quality for drinking in both seasons. These findings highlight the critical need for authorities and decision-makers to adopt effective protection strategies to safeguard groundwater resources and promote their long-term sustainability. This study provides an initial insight into seasonal contrasts but does not replace long-term monitoring. Additional investigations are needed to understand the underlying process governing the long-term seasonal variations of the groundwater quality. A full sozological analysis is recommended for future work to strengthen groundwater contamination source attribution and quantify anthropogenic vs. climatic contributions.

REFERENCES

Abanyie, S.K., Apea, O.B., Abagale, S.A., Amuah, E.E.Y., Sunkari, E.D., 2023. Sources and factors influencing groundwater quality and associatedhealth implications: A review. Emerging Contaminants 9(2), 100207.

Abbasi, N., Zarin, R., Raziq, A., Al-Quraishi, A.M.F., 2024. Remote sensing, artificial neural networks, and spatial interpolation methods for modelling soil chemical characteristics. Modeling Earth Systems and Environment 10, 5063–5078. https://doi.org/10.1007/s40808-024-02050-y

Agoubi, B., Kharroubi, A., Abida, H., 2013. Saltwater intrusion modelling in Jorf coastal aquifer, Southeastern Tunisia: geochemical, geoelectrical and geostatistical application. Hydrological Processes 27, 1191–1199.

Alzahrani, A., Basaloom, A., Mosaad, S., 2025. Geochemical-based appraisal of karst groundwater quality, west Nile Valley, central Egypt, for drinking and irrigation. Journal of Hydrology: Regional Studies 57, 102152.

APHA, 1992. Standard methods for the examination of water and wastewater. In: American Water Works Association (AWWA) and Water Pollution Control Federation (WPCF), 18. American Public Health Association (APHA), Washington DC. https://betastatic.fishersci.com/content/dam/fishersci/en_US/documents/programs/scientific/technical-documents/white-papers/apha-water-testing-standa rd-methods-introduction-white-paper.pdf

Arslan, H., 2012. Spatial and temporal mapping of groundwater salinity using ordinary kriging and indicator kriging: The case of Bafra Plain, Turkey. Agricultural Water Management 113, 57–63.

Askri, B., Ahmed, A.T., Bouhlila. R., 2022. Origins and processes of groundwater salinisation in Barka coastal aquifer, Sultanate of Oman. Physics and Chemistry of the Earth 126, 103116. https://doi.org/10.1016/j.pce.2022.103116

Ayadi, Y., Mokadem, N., Besser, H., Redhaounia, B., Khelifi, F., Harabi, S., Nasri, T., Hamed, Y., 2018. Statistical and geochemical assessment of groundwater quality in Teboursouk area (Northwestern Tunisian Atlas). Environmental Earth Sciences 77, 1–20. https://doi.org/10.1007/s12665-018-7523-2

Ayed-Khaled, A, Zouaghi, T, Ghanmi, M., 2017. Structural dynamics in northern Atlas of Tunisian, Jendouba area: insights from geology and gravity data. Journal of Tethys 5, 103–114.

Batarseh, M., Imreizeeq, E., Tilev, S., Al Alaween, M., Suleiman, W., Al Remeithi, A.M., Al Tamimi, M.K., Al Alawneh, M., 2021. Assessment of groundwater quality for irrigation in the arid regions using irrigation water quality index (IWQI) and GIS-Zoning maps: Case study from Abu Dhabi Emirate, UAE. Groundwater for Sustainable Development, 14, 100611.

Belhadj, C., Riahi, R., Sebei, A., Sifi, S., Rebai, N., 2025. Advanced groundwater potential and contamination vulnerability assessment using integrated GIS-based AHP techniques: A case study from the Bizerte watershed, Tunisia. Environmental and Sustainability Indicators 26, 100597.

Ben Ayed, L., Horry, M., Sabbahi, S., Nouiri, I., Karanis, P., 2022. Physico-chemical quality of the Medjerda River in Tunisia and suitability for irrigation during the moist and the dry seasons. Bulletin de la Société Royale des Sciences de Liège 91, 23–43. https://doi.org/10.25518/0037-9565.10857

Benyoussef, S., Arabi, M., El Yousfi, Y., Makkaoui, M., Gueddari, H., El Ouarghi, H., Abdaoui, A., Ghalit, M., Zegzouti, Y.F., Azirar, M., Himi, M., Alitane, A., Chahban, M., Boughrous, A.A., 2024. Assessment of groundwater quality using hydrochemical process, GIS and multivariate statistical analysis at central Rif, North Morocco. Environmental Earth Sciences 83, 515. https://doi.org/10.1007/s12665-024-11798-6

Bouita, M., El mahdi, Y., Sbai, H., Bouita, I., El bakouri, A., Ibrahimi, E.M., Chakir, E.M., 2021. Assessment of nitrogen pollution of groundwater in the Maamora Gharb aquifer, Morocco. Egyptian Journal of Aquatic Biology and Fisheries 25, 739–758.

Chaudhary, I.J. Chauhan, R., Kale, S.S., Gosavi, S., Rathore, D., Dwivedi, V., Singh, S., Yadav, V.K., 2025. Groundwater Nitrate Contamination and its Effect on Human Health: A Review. Water Conservation Science and Engineering 10(33). https://doi.org/10.1007/s41101-025-00359-y

Davamani, V., John, J.E., Poornachandhra, C., Gopalakrishnan, B., Arulmani, S., Parameswari, E., Santhosh, A., Srinivasulu, A., Lal, A., Naidu, R., 2024. A critical review of climate change impacts on groundwater resources: a focus on the current status, future possibilities, and role of simulation models. Atmosphere 15, p. 122.

DGRE, 2020a, Situation de l'exploitation des nappes phréatiques de la Tunisie. Direction Générale des Ressources en Eau, Tunis. 133p

DGRE, 2020b. Annuaire de l'exploitation des nappes profondes de la Tunisie. Direction Générale des Resources en Eau, Tunis.

Gaaloul, N., Eslamian, S., Katlane, R., 2023. Socio economic impacts of Hydrological Hazards and Disasters in Tunisia. International Journal Water Sciences and Environment Technologies 8, 17–49.

Hadroug, S., Khiari, B., Jellali, S., El-Bassi, L., Al-Wardy, M., Hamdi, W., Jeguirim, M., 2025. Animal manure derived biochars synthesis, characterization and use for wastewater treatment and in agriculture: A recent review. Science of The Total Environment 985, 179751, 0048–9697. https://doi.org/10.1016/j.scitotenv.2025.179751

Hamdi, W., Beji, R., Ouertatani, S., Gharbi, A., 2018. Effect of Nitrogen and Potassium Levels on the Potatoes Growth in the Chott Mariem Region of Tunisia. Journal of Experimental Agriculture International 28(5), 1–9. https://doi.org/10.9734/JEAI/2018/20206

Hamdi, W., Hamdi, N., Jellali, S., Seffen, M., 2022. Effect of background electrolytes on the adsorption of phosphorus (P) onto southern Tunisia natural clays. Physics and Chemistry of the Earth, Parts A/B/C, 127, 103160. https://doi.org/10.1016/j.pce.2022.103160

Hamed, Y., Redhaounia, B., Ben Sâad, A., Hadji, R., Zahri, F., 2017. Groundwater Inrush Caused by the Fault Reactivation and the Climate Impact in the Mining Gafsa Basin (Southwestern Tunisia). Journal of Tethys 5, 154–164.

Irvine, D.J., Singh, K., Kurylyk, B.L., Briggs, M.A., Sebastian, Y., Tait, D.R., Helton, A.M., 2024. Groundwater-Surface water interactions research: Past trends and future directions. Journal of Hydrology 644, 132061.

Kadir, M., Fehri, R., Souag, D., Vanclooster, M., 2020. Exploring causes of streamflow alteration in the Medjerdariver, Algeria. Journal of Hydrology: Regional Studies 32, 100750.

Karunanidhi, D.,Aravinthasamy, P., Subramani, T., Setia, R., 2021.

Groundwater suitability estimation for sustainable drinking water supply and food production in a semi-urban area of south India: A special focus on risk evaluation for making healthy society. Sustainable Cities and Society 73, 103077.

Katz, B.G., Eberts, S.M., Kauffman, L.J., 2011. Using Cl/Br ratios and other indicators to assess potential impacts on groundwater quality from septic systems: A review and examples from principal aquifers in the United States. Journal of Hydrology 397, 151–166.

Lissir, B., Louhichi, B., Mabrouk, A., Salem Abdennaji, T., Hamdi, W., Hamdi, N., Houas, A., 2025. A Study of an Experimental Design Methodology for the Removal of Cadmium from Polluted Wastewater via the Electrocoagulation Process using Solar Energy. Engineering, Technology & Applied Science Research 15(3), 23415–23421. https://doi.org/10.48084/etasr.9634

Liu, G., Gao, M., Zhu, M., Ren, S., Fan, J., 2025. Analysis of the Quality of Typical Acidic Groundwater of the Guangwang Mining Area and Its Associated Human Health Risks. Sustainability 17, 2677. https://doi.org/10.3390/su17062677.liu

Maman Hassan, A., Fırat Ersoy, A., 2022. Hydrogeochemical and isotopic investigations on the origins of groundwater salinization in Çarşamba coastal aquifer (North Turkey). Environmental Earth Sciences 81, 128. https://doi.org/10.1007/s12665-022-10248-5.

Macdonald, B.C.T., Nachimuthu, G., Chang, Y.F., Nadelko, A.J., Tuomi, S., Watkins, M., 2020. Nitrogen composition in furrow irrigated run-off water. Agricultural Water Management 242, 106399. https://doi.org/10.1016/j.agwat.2020.106399

Moussaoui, Z., Gentilucci, M., Wederni, K., Hidouri, N., Hamedi, M., Dhaoui, Z., Hamed, Y., 2023. Hydrogeochemical and Stable Isotope Data of the Groundwater of a Multi-Aquifer System in the Maknessy Basin (Mediterranean Area, Central Tunisia). Hydrology 10, 32. https://doi.org/10.3390/hydrology10020032

Nives, Š.G., 1999. Water quality evaluation by index in Dalmatia. Water Research 33, 3423–3440.

Nong, X., Shao, D., Zhong, H., Liang, J., 2020. Evaluation of water quality in the South-to-North Water Diversion Project of China using the water quality index (WQI) method. Water Research 178, 115781.

Nyika, J., Magnone, D., Gould, I., 2024. Groundwater salinization challenges in agriculturally valuable low-lying North Sea region: A review. Cleaner Water 2, 100052.

Parkhurst, D.L., Appelo, C.A.J., 1999. User's guide to PHREEQC (version 2) – a computer program for speciation, batch-reaction, one-dimensional transport, and inverse geochemical calculations. Water-Resources Investigations Report USGS, 99–4259. https://doi.org/10.3133/wri994259

Piper, A.M., 1944. A Graphical interpretation of water-analysis. Transactions of the American Geophysical Union 25, 914–928. https://doi.org/10.1029/TR025i006p00914

Rajosoa, A.S., Abdelbaki, C., Mourad, K.H., 2022. Assessing the impact of climate change on the Medjerda River Basin. Arabian Journal of Geosciences 15, 1–9. https://doi.org/10.1007/s12517-022-10288-y

Rouhani, A., Ben-Salem, N., D'Oria, M., Silva, R.C.G., Viglione, A., Copty, N.K., Barry, A., Gómez-Hernández, J.J., Jomaa, S., 2025. Direct impact of climate change on groundwater levels in the Iberian Peninsula. Science of The Total Environment 970, 179009.

Sampath, V.K., Radhakrishnan, N., 2022. A comparative study of LULC classifers for analysing the cover management factor and support practice factor in RUSLE model. Earth Science Informatics 6, 733–751.

Sanad, H., lhaj, M.O., Zouahri, A., Saafadi, L., Dakak, H., Mouhir, L., 2024. Groundwater pollution by nitrate and salinization in Morocco: a comprehensive review. Journal of Water and Health 22, 1756–1773.

Serrano, L., Díaz-Paniagua, C., Gómez-Rodríguez, C., Florencio, M., Marchand, M.A, Roelofs, J.G.M., Lucassen, E.C., 2016. Susceptibility to acidification of groundwater-dependent wetlands affected by water level declines, and potential risk to an early-breeding amphibian species. Science of The Total Environment 571, 253–1261: 0048–9697. https://doi.org/10.1016/j.scitotenv.2016.07.156.

Singh, S., Ghosh, N.C., Gurjar, S., Krishan, G., Kumar, S., Barwal, P., 2018. Index-based assessment of suitability of water quality for irrigation purpose under Indian conditions. Environment Monitoring and Assessment 190, 29. https://doi.org/10.1007/s10661-017-6407-3.

Slimani, F.Z., Zghibi, A., Elomri, A., Aloui, S., Naeem, K., Merzougui, A., Msaddek, M.H., Chekirbene, A., 2024. Identification of groundwater potential recharge zones in a Tunisian anthropogenic coastal region: Insights from multi-criteria decision-making techniques. Journal of African Earth Sciences 209, 105108.

Tlili-Zrelli, B., Gueddari, M., Bouhlila, R., 2018. Spatial and Temporal Variations of Water Quality of Mateur Aquifer (Northeastern Tunisia): Suitability for Irrigation and Drinking Purposes. Journal of Chemistry 2090–9063, https://doi.org/10.1155/2018/2408632

Tyagi, S., Sharma, B., Singh, P., Dobhal, R., 2013. Water quality assessment in terms of water Quality Index. America Journal of water Resources 1, 34–38. https://doi.org/10.12691/ajwr-1-3-3.

Uddin, Md G., Nash, S., Olbert, A.I., 2021. A review of water quality index models and their use for assessing surface water quality. Ecological Indicators 122, 107218.

World Health Organization (WHO), 2022. Guidelines for drinking-water quality: incorporating the first and second addenda. WHO, Geneva.

Yıldız, S., Karakuş, C.B., 2020. Estimation of irrigation water quality index with development of an optimum model: a case study. Environ Dev Sustain 22, 4771–4786. https://doi.org/10.1007/s10668-019-00405-5.